Methodology of an optical pump-terahertz probe experiment: An analytical frequency-domain approach

H. Němec, F. Kadlec, and P. Kužel
Institute of Physics, Academy of Sciences of the Czech Republic, and Center for Molecular Systems and Biomolecules, Na Slovance 2, 182 21 Prague 8, Czech Republic

(Received 19 March 2002; accepted 15 August 2002)

Time-resolved optical pump-terahertz (THz) probe experiments are currently used to obtain information about the ultrafast dynamics of photoexcited carriers in semiconductors and about the far-infrared nonlinear response during solvation in liquids. The THz dynamics in such photoexcited systems is fully characterized by a two-dimensional nonlinear susceptibility. We have developed a frequency-domain analytical method for the direct extraction of this susceptibility from the experimental data. Following effects are taken into account: dispersive propagation of radiation in a photoexcited medium, refraction on its surfaces, THz sensor responsivity, and spatio-temporal transformations of the THz pulses. Strategies for possible experiments are discussed. © *2002 American Institute of Physics.* [DOI: 10.1063/1.1512648]

I. INTRODUCTION

Recent technological developments have made it possible to optimize methods of emission and detection of ultrashort THz pulses and thus to obtain an experimental dynamic range of the order of up to about 80 dB for the transmission measurements of steady equilibrium states.[1] This increased performance of THz experiments along with the possibility of a coherent phase-sensitive detection enables this technique to supplement and, in many cases, to improve information obtained by classical far-infrared spectroscopy. The THz spectroscopy is based on analysis of a recorded temporal profile of the electric field of a broadband THz pulse transmitted through the investigated sample and yields its complex transmission spectrum in the submillimeter spectral range (typically 2–80 cm^{-1}). The technique involves optically gated emission and detection of the THz pulses, and consequently, it is well suited for time-resolved transmission experiments of nonequilibrium states (with subpicosecond resolution), for which the classical spectroscopic techniques cannot be used. This feature has lead to the development of the optical pump-THz probe (OPTP) experiments in which the broadband THz pulses are used to probe far-infrared changes of the susceptibility spectrum initiated by an optical excitation event. Unlike the usual optical pump-optical probe experiments, the OPTP technique allows observation of the evolution of the entire THz probe waveform as a function of the negative delay of the optical pump pulse.[2] Thus, as long as the optically induced changes in the far-infrared spectrum are sufficiently strong, two-dimensional (2D) temporal scans can be carried out in order to provide complete information about the system dynamics. A number of papers have been devoted to the study of photocarrier dynamics in semiconductors[3–11] and superconductors[12] by the OPTP technique. In these previous experiments, the free carrier absorption represents the principal interaction of the THz radiation with the sample. Therefore the transmitted intensity of the THz probe is sensitive mainly to the time-dependent free-carrier concentration and 2D temporal scans can be performed with sufficient sensitivity because adequate photocarrier concentrations can be easily generated by a high-intensity pump pulse.[9] However, it still remains a challenge to study the photochemical processes, namely, solvation dynamics and photo-induced environmental relaxation,[13–15] because here the optically induced changes are very small.

In the OPTP experiments, the THz pulse directly probes picosecond or subpicosecond dynamics, i.e., the nonequilibrium temporal evolution of the studied system involves frequency components falling into (or overlapping with) the THz range. This may produce a frequency mixing which can lead to interesting changes in the THz waveform. This requires an appropriate and a very careful analysis of the experimental data in order to avoid artifacts.[12]

Recently, an analytical theory was developed to describe the time-dependent response function for OPTP experiments.[2] An appropriate methodology of the experiment was proposed, one of its major points being a proper definition of the times involved in the experimental scans. This theory describes a weak secondary THz waveform related to the nonequilibrium part of the dielectric susceptibility $\Delta\chi$ and allows extraction of $\Delta\chi$ from the experiment without any *a priori* model of nonequilibrium behavior. However, this theory does not take into account the contribution of the interfaces between the nonequilibrium medium and the surrounding space; this contribution becomes significant for samples which are thin or which absorb strongly in the optical or THz range. On the other hand, this theory can fail also for thick samples since it implicitly assumes a perfect velocity matching of the pump and probe pulse. Also, it does not take into account waveform transformations due to the free-space propagation nor the detection process and thus it cannot be used directly to interpret the experimental data.

An alternative way of the OPTP data treatment uses the numerical method of finite-difference time-domain (FDTD) calculations[11,15] which simulates the propagation of the THz

pulse through the nonequilibrium medium with a known dielectric response. The advantage of this method is that it can take into account all nonequilibrium effects; in particular it can model situations when the modifications of the THz field are strong and cannot be described using a perturbative approach. On the other hand, the FDTD method was not designed for the solution of the inverse problem, i.e., the extraction of $\Delta\chi$ is not straightforward. It requires an *a priori* explicit model for nonequilibrium behavior, the parameters of which are to be adjusted using FDTD calculations.

The authors of both of the above theories work in the time domain and conclude that it is not possible to use Fourier transform (FT) methods for the description of OPTP experiments: the principal difficulty arises from the fact that the properties of the studied photoexcited medium change quickly compared to the frequency of the probing radiation. On the other hand, FT methods are an excellent tool widely used for the interpretation of steady-state THz transmission experiments;[1,16,17] they avoid a large number of experimental errors that arise if the time-domain approach is applied (see Sec. II). Thus, taking into account the experimental difficulty of the OPTP experiments, it would be very convenient to have a methodology that would enable applying FT formalism at least partially. The aim of this paper is to propose such a formalism and to discuss its application. Using 2D FT we have developed an analytical model which handles to the first order all nonequilibrium effects, including the refraction on the surfaces of a photoexcited medium, dispersion, THz/optical velocity mismatch and pump intensity extinction. We have obtained an explicit formula for the nonequilibrium part of the susceptibility which can be applied to free-carrier dynamics in semiconductors as well as to solvation dynamics in liquids. The best strategies for the experiment can be then proposed. The paper is structured as follows: in Sec. II we will compare the FT approach to that of the time-domain; in Sec. III we will develop the FT formalism applicable to the OPTP experiments; Sec. IV is then devoted to the solution of the electromagnetic propagation in a photoexcited medium, and finally, in Sec. V we will discuss how to perform the experiment and how to deal with the data within these approaches.

II. COMPARISON OF THE TIME-DOMAIN AND FREQUENCY-DOMAIN METHODS

The THz photoconductive[18] or electro-optic[19] sampling is a phase-sensitive detection method which makes it possible to measure and evaluate the THz electric field as a function of time. Strictly speaking, if $E^E(t)$ is the true near-field THz waveform emitted by an emitter (see Fig. 1), then, within the linear electromagnetic theory, the experimental signal $E^D(t)$ delivered by the sensor is equal to:

$$E^D(t) = E^E(t) * \psi(t), \tag{1}$$

where the asterisk represents a convolution. The response function $\psi(t)$ describes the detection process and the changes of the THz pulse shape due to the propagation. Namely, this function accounts for:

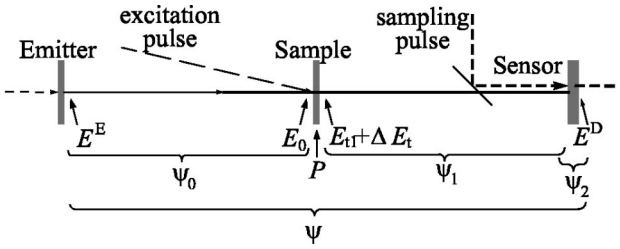

FIG. 1. Propagation of a THz pulse from the emitter to the detector; schematic definitions of instrumental functions.

(1) A distortion of the THz waveform due to the propagation through dispersive media, e.g., a sample for transmission measurements[17,20] or water vapor present in the atmosphere;[21]
(2) A substantial reshaping of the THz pulse owing to the free-space propagation of a spatially limited broadband beam,[22] and due to the focusing optics and its finite aperture;[23,24]
(3) A detection process itself. It should include the characteristics of the optical sampling pulse and, e.g., in the case of electro-optic sampling, the dispersion properties of the Pockels crystal both in optical and in THz spectral range.[25,26]

All these points should be taken into account for the THz emission experiments,[27] where the exact shape of the emitted waveform has to be recovered from the measured one. It should be emphasized that reshaping due to propagation is a significant effect which can be hardly accounted for precisely by calculation, except when no focusing optics is used.

The usual THz transmission experiments use the FT to eliminate an unknown response function and emitted waveform $E^E(t)$ through the convolution theorem. The spectroscopic method consists in a measurement of a reference waveform $E_r(t)$ with an empty diaphragm and a signal waveform $E_s(t)$ with the sample attached to the diaphragm and filling the whole aperture. Let the response functions $\psi_0(t)$, $\psi_1(t)$, and $\psi_2(t)$ describe the evolution of the waveform before the sample (ψ_0), its evolution after the sample (ψ_1), and the detector response (ψ_2) (see Fig. 1). Let $T_s(t)$ describe the transmission through the sample of a thickness d, and $T_0(t)=\delta(t-d/c)$ (Dirac δ-function) be the transmission through the air slab of an equal thickness (empty diaphragm). One can then write in the Fourier space,

$$\frac{E_s^D(\omega)}{E_r^D(\omega)} = \frac{\psi_2(\omega)\cdot\psi_1(\omega)\cdot T_s(\omega)\cdot\psi_0(\omega)\cdot E^E(\omega)}{\psi_2(\omega)\cdot\psi_1(\omega)\cdot T_0(\omega)\cdot\psi_0(\omega)\cdot E^E(\omega)} = \frac{T_s(\omega)}{T_0(\omega)}. \tag{2}$$

The unknown response functions are thus eliminated and the measured signal is related only to the properties of the sample. We now emphasize that the sample properties are obtained only within a well defined frequency range where both $E_s^D(\omega)$ and $E_r^D(\omega)$ significantly exceed the noise level. This range is narrower than the bandwidth initially transmitted by the THz field $E^E(\omega)$ due to a possible high absorption

of the sample and due to the frequency dependence of ψ_0, ψ_1, and ψ_2. The time-domain response function $T_s(t)$ obtained from the measured $T_s(\omega)$ through the inverse FT is then always distorted since some parts of the spectra are inaccessible.

The authors of Ref. 2 carefully described the OPTP experiment, however the direct application of their theory leads to an emissionlike experiment; the sample which is represented here by dissolved chromophores in a cuvette becomes the source of a secondary THz radiation due to the polarization induced by the incident THz pulse. Within this treatment the evaluation of the polarization motion in the sample and, consequently, of the near THz field is direct, however, the waveform which can be obtained experimentally has a shape completely different from the true waveform in the near field due to ψ_1. Specifically, the measurements should be performed in the far field without any focusing optics,[27–29] as the reshaping due to focusing depends on the geometrical parameters of the experimental setup (distances, mirror sizes, angles, etc.);[23] these changes could hardly be taken into account in all detail. This condition makes it more difficult to use photoconductive antennas with a small gap between electrodes owing to the presence of a spherical lens which precedes such an antenna, and which serves to collect the signal into the active area: this lens should be removed for these experiments.[30] In any case, the detector response ψ_2 should be very carefully evaluated and taken into account, and the true waveform of the THz pulse impinging on the sample should be determined. Otherwise, a systematic error will be introduced into the evaluation of the studied phenomena, viz., the precision of this evaluation will be limited by uncertainties in ψ_0.

All these problems will be discussed further in subsequent sections within the frame of the FT formalism which allows to eliminate partially the unknown response functions.

III. FORMULATION OF THE PROBLEM

A. Nonlinear polarization

The propagation of the THz probe pulse through the studied sample is coupled to a THz polarization wave which emits a secondary THz pulse that will be detected. The process under investigation is nonlinear; the THz nonequilibrium response at some point of the photoexcited medium can be described using the third order nonlinear susceptibility $\tilde{\chi}^{(3)}$. The nonlinear contribution ΔP to the total polarization P can be written using the formula,

$$\Delta P(t)=\varepsilon_0 \int\int\int \tilde{\chi}^{(3)}(t',t'',t''')E_{\mathrm{opt}}(t-t''') \times E_{\mathrm{opt}}(t-t'')(E_{\mathrm{THz}}(t-t')dt'dt''dt''', \quad (3)$$

which describes a coupling between the field E_{opt} of the optical pump pulse, and the total THz electric field E_{THz}. Such an expression is valid at each point of the sample, however, the shape of the electric fields can vary due to dispersion and absorption. Nevertheless, we assume that the optical pulse is much shorter than characteristic times of interactions that can be studied using available THz pulses. Then Eq. (3) becomes

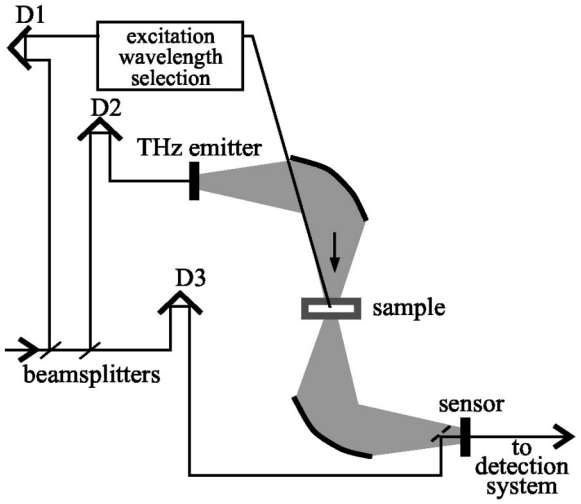

FIG. 2. Scheme of the experimental setup of OPTP experiments; D1, D2, D3: delay lines.

$$\Delta P(t,t-t_e)=\varepsilon_0 \int_{-\infty}^{t} E_{\mathrm{THz}}(t')\Delta\chi(t-t',t-t_e)dt', \quad (4)$$

where t_e marks the time of the optical excitation, and t is the time when we look at the value of the polarization ΔP (through the emitted secondary THz pulse). The generalized susceptibility $\Delta\chi$ depends on two time variables: the first one is related to the dielectric response to a probe pulse, and the second one describes the influence of the optical excitation,

$$\Delta\chi(t',t-t_e)\equiv I_{\mathrm{opt}} \int\int \tilde{\chi}^{(3)}(t',t'',t''')\delta(t-t'''-t_e) \times \delta(t-t''-t_e)dt''dt''' = I_{\mathrm{opt}}\tilde{\chi}^{(3)}(t',t-t_e,t-t_e). \quad (5)$$

Up to now the THz probe pulse arrival was defined only implicitly through the general form of $E_{\mathrm{THz}}(t')$ in Eq. (4). However, in the experiment, the delays of all pulses—excitation, probe, and sampling—can be independently controlled. For clarity, we introduce a time t_p describing the THz probe pulse arrival. When the time origin is shifted by t_p, Eq. (4) becomes

$$\Delta P(t-t_p,t-t_e) = \varepsilon_0 \int_{-\infty}^{t-t_p} E_{\mathrm{THz}}(t')\Delta\chi(t-t_p-t',t-t_e)dt'. \quad (6)$$

After a substitution Eq. (6) takes this form,

$$\Delta P(t-t_p,t-t_e)=\varepsilon_0 \int_{-\infty}^{t} E_{\mathrm{THz}}(t'-t_p)\Delta\chi(t-t',t-t_e)dt', \quad (7)$$

which allows explicitly to delay the incident THz waveform in time through t_p.

B. Definition of representations following experimental schemes

Experimentally, one can control the position of the three delay lines as shown in Fig. 2. The delay line 1 (D1) deter-

mines the pump pulse arrival (i.e., time t_e), line 2 (D2) controls the delay of the THz probe pulse, i.e., its position is related to time t_p, and line 3 (D3) allows to scan the shape of the freely propagating THz waveform (i.e., time t). As the probe-pulse profile is not a δ-function, the time t_p can be more or less arbitrarily chosen; however, during the experiment, t_p is connected to a definite position of D2.

It is convenient to define relative delay times: pump–probe delay $\tau_p = t_p - t_e$, pump–sampling (=measurement) delay $\tau_e = t - t_e$, and probe–measurement delay $\tau = t - t_p$. During a 2D scan two delay lines are mobile and the remaining one is held in a fixed position. Following their choice, two of the above defined delays can be treated as independent variables:

(i) D3 is fixed: D1 scans τ_e and D2 scans τ (both in a negative direction);
(ii) D2 is fixed: D1 changes τ_p (in a negative direction) and D3 corresponds to τ;
(iii) D1 is fixed: D2 corresponds to τ_p and D3 to τ_e.

The natural choice of the reference waveform is a signal obtained as a transmission through a non-excited sample in equilibrium (i.e., the pump beam is suppressed). For this measurement only the delay time τ has a physical sense; its change can be achieved through the shift of either D2 or D3. Consequently, the 2D scan denoted above as (III) would not be a suitable choice since it has no connection to this reference: for the sake of simplicity, it will be omitted in the following analysis. We are thus left with two possibilities, how to select the pair of independent delays for 2D scans. Following the choice of the proper variables we can define two representations for polarization and susceptibility. We denote by the superscript (I) the representation where τ and τ_e are chosen as proper variables, and by (II) the representation with proper variables τ and τ_p. These representations are simply related by the expression,

$$A^{(I)}(\tau,\tau_e) = A^{(II)}(\tau,\tau_p=\tau_e-\tau), \tag{8}$$

i.e., the quantity A has the same value in both representations given the position of the three delay lines; on the other hand, the mathematical form of the functions $A^{(I)}$ and $A^{(II)}$ is in general different. We obtain then for the polarization change,

$$\Delta P^{(I)}(\tau,\tau_e) = \varepsilon_0 \int_{-\infty}^{\tau} E_{THz}(t')\Delta\chi^{(I)}(\tau-t',\tau_e)dt', \tag{9a}$$

$$\Delta P^{(I)}(\tau,\tau_e) = \varepsilon_0 \int_{-\infty}^{\tau} E_{THz}(t')\Delta\chi^{(II)}(\tau-t',\tau_e-\tau+t')dt', \tag{9b}$$

$$\Delta P^{(II)}(\tau,\tau_p) = \varepsilon_0 \int_{-\infty}^{\tau} E_{THz}(t')\Delta\chi^{(I)}(\tau-t',\tau_p+\tau)dt', \tag{9c}$$

$$\Delta P^{(II)}(\tau,\tau_p) = \varepsilon_0 \int_{-\infty}^{\tau} E_{THz}(t')\Delta\chi^{(II)}(\tau-t',\tau_p+t')dt'. \tag{9d}$$

It should be emphasized that $\Delta\chi^{(I)}$ and $\Delta\chi^{(II)}$ describe the same physical process and bear the same information about it; however, their mathematical form is different as they are expressed using different proper variables.

C. Transformation into the frequency space

As will be shown in the next section, the application of the FT to a single variable, whether it be τ, τ_p or τ_e, always leads to an integral relation between the measured THz electric field E^D and $\Delta\chi$. However, the application of the 2D FT leads to simpler results in all cases. We use the following definition of the FT,

$$A(\Omega) = \int_{-\infty}^{\infty} A(t)\exp(-i\Omega t)dt,$$

which implies that the refractive indices in the media with losses will have a negative imaginary part: $N = n - i\kappa$. Let us denote the angular frequencies conjugated to delays τ, τ_e, and τ_p as ω, ω_e, and ω_p, respectively. Then, a 2D FT applied for example to a quantity $A(\tau,\tau_e)$ in the representation (I) is defined as

$$A(\omega,\omega_e) = \int_{-\infty}^{\infty}\int_{-\infty}^{\infty} A(\tau,\tau_e)\exp(-i\omega\tau) \times \exp(-i\omega_e\tau_e)d\tau d\tau_e.$$

The application of the 2D FT to Eqs. (9a), (9b), (9c), (9d) leads after a straightforward calculation to

$$\Delta P^{(I)}(\omega,\omega_e) = \varepsilon_0 E_{THz}(\omega)\Delta\chi^{(I)}(\omega,\omega_e), \tag{10a}$$

$$\Delta P^{(I)}(\omega,\omega_e) = \varepsilon_0 E_{THz}(\omega)\Delta\chi^{(II)}(\omega+\omega_e,\omega_e), \tag{10b}$$

$$\Delta P^{(II)}(\omega,\omega_p) = \varepsilon_0 E_{THz}(\omega-\omega_p)\Delta\chi^{(I)}(\omega-\omega_p,\omega_p), \tag{10c}$$

$$\Delta P^{(II)}(\omega,\omega_p) = \varepsilon_0 E_{THz}(\omega-\omega_p)\Delta\chi^{(II)}(\omega,\omega_p). \tag{10d}$$

Note the frequency mixing appearing in some terms of Eqs. (10b), (10c), (10d); mathematically, this is a direct consequence of the fact that, while the relation (9a) represents a convolution in the variable τ, the relations (9b)–(9d) are not true convolutions. Physically, this is related to the absence of the translational symmetry in time by reason of the excitation. In other words, the end of the terahertz pulse (which arrives after the excitation) experiences a different response than its beginning: new spectral components can be generated as a consequence of the dynamics of $\Delta\chi$.

We will also need to know the 2D FTs of time convolutions of some function $\psi(t)$ with ΔP (or with THz electric field) in both representations [cf. Eq. (1)]. Since the convolution involves variable t we can write it in the form,

$$\Delta P^{(I)}(\tau,\tau_e) * \psi(t) = \int_{-\infty}^{\infty} \Delta P^{(I)}(t-t'-t_p, t-t'-t_e)\psi(t')dt' = \int_{-\infty}^{\infty} \Delta P^{(I)}(\tau-t',\tau_e-t')\psi(t')dt', \tag{11a}$$

$$\Delta P^{(\mathrm{II})}(\tau,\tau_p)*\psi(t)=\int_{-\infty}^{\infty}\Delta P^{(\mathrm{II})}(t-t'-t_p,t_p-t_e)\psi(t')dt'$$

$$=\int_{-\infty}^{\infty}\Delta P^{(\mathrm{II})}(\tau-t',\tau_p)\psi(t')dt'. \quad (11b)$$

The 2D FTs of these expressions then lead to

$$FT(\Delta P^{(\mathrm{I})}(\tau,\tau_e)*\psi(t))=\psi(\omega+\omega_e)\Delta P^{(\mathrm{I})}(\omega,\omega_e), \quad (12a)$$

$$FT(\Delta P^{(\mathrm{II})}(\tau,\tau_p)*\psi(t))=\psi(\omega)\Delta P^{(\mathrm{II})}(\omega,\omega_p). \quad (12b)$$

IV. SOLUTION OF THE WAVE EQUATION FOR A PHOTOEXCITED SAMPLE

A. General considerations

We consider a sample of thickness L surrounded by media with refractive indices n_1 (before the sample) and n_2 (after the sample). It can be, e.g., air or cuvette material; we consider the most general case where the two media can be different. In equilibrium, the sample is assumed to be a homogeneous slab with two flat and parallel surfaces and a refractive index N; in the time domain it is characterized by the dielectric response function ε. All the indices n_1, n_2, and N may be complex and frequency-dependent. Let us denote $E_0(t,\ z)$ the THz pulse coming into the sample under normal incidence. To be precise, $E_0(t,\ z=0^+)$ is the THz wave which has just been transmitted through the input interface (air/sample or cuvette/sample) according to equilibrium Fresnel equations. It is assumed to be a plane wave. In the following we also suppose that it is possible to proceed to the temporal windowing of the THz signal in order to cut the internal Fresnel reflections in the sample: these are not considered in the main part of this paper, however, they are treated in the Appendix. In the photoexcited state the total THz field $E_{\mathrm{THz}}(t,\ z)$ in the sample is equal to

$$E_{\mathrm{THz}}(t,z)=E_0(t,z)+\Delta E_1(t,z), \quad (13)$$

where ΔE_1 is a secondary THz wave induced by the nonlinear polarization $\Delta P(t,\ t-t_e,\ z)$. From now on, we assume that the secondary field ΔE_1 is small compared to the primary one, E_0. This is the most important assumption of our model which allows to linearize it. It is justified in many practical cases; $\Delta\chi$ scales linearly with the incoming optical fluence I_{opt} [cf. Eq. (5)], and consequently the magnitude of ΔE_1 can be limited in the experiment. However, if interactions at a very high excitation density are to be studied (e.g., investigation of the carrier screening in semiconductors at high photocarrier densities) this model cannot be applied. Within the above approximation, ΔP can be written in the following form:

$$\Delta P(t,t-t_e,z)=\varepsilon_0\int_{-\infty}^{t}E_0(t',z)\exp(-\alpha z)$$

$$\times\Delta\chi(t-t',t-(t_e-z/v_g))dt', \quad (14)$$

where we replaced the total THz field by the primary one, the propagation of which is well known. In addition, we explicitly accounted for the absorption of the optical beam through the coefficient α, and for its group velocity of propagation in the sample (v_g). Within the above mentioned approximation, the wave equation for ΔE_1 can be written as

$$\frac{\partial^2\Delta E_1}{\partial z^2}-\frac{1}{c^2}\frac{\partial^2}{\partial t^2}(\varepsilon*\Delta E_1)=\mu_0\frac{\partial^2\Delta P}{\partial t^2}. \quad (15)$$

The dispersion of the secondary waveform is accounted for by the linear (equilibrium) time domain response function ε.

B. Input interface

We may now pass to the variables τ and τ_e or τ and τ_p, and transform the wave equation into frequency space. We apply the 2D FT to both sides of Eq. (15) and using Eqs. (10a), (10d) and (12a), (12b) we get

$$\frac{d^2\Delta E}{dz^2}+k_1^2\Delta E=-k_0^2e_0\exp(-iK_Fz), \quad (16)$$

where $\Delta E(\omega,\omega_e)$ in representation (I) or $\Delta E(\omega,\omega_p)$ in representation (II) are the 2D FTs of $\Delta E_1(\tau,\tau_e)$ or $\Delta E_1(\tau,\tau_p)$, respectively. The other symbols used in expression (16) have the following definitions for the two representations:

Representation I:

$$k_1=\frac{(\omega+\omega_e)N(\omega+\omega_e)}{c},\quad k_0=\frac{\omega+\omega_e}{c},$$

$$K_F=\frac{\omega N(\omega)}{c}+\frac{\omega_e}{v_g}-i\alpha,$$

$$e_0=E_0(\omega,z=0^+)\Delta\chi^{(\mathrm{I})}(\omega,\omega_e),$$

Representation II:

$$k_1=\frac{\omega N(\omega)}{c},\quad k_0=\frac{\omega}{c},$$

$$K_F=\frac{(\omega-\omega_p)N(\omega-\omega_p)}{c}+\frac{\omega_p}{v_g}-i\alpha,$$

$$e_0=E_0(\omega-\omega_p,z=0^+)\Delta\chi^{(\mathrm{II})}(\omega,\omega_p).$$

As all the equations are analogous for the two representations, we will pursue the calculation for representation II only and we will present the results for representation I at the end of this section. We would like to emphasize that in representation II, $\omega-\omega_p$ has the meaning of the frequency of the primary THz wave E_0: this wave drives the component ΔE of the secondary wave which oscillates at the frequency ω and it is parametrized by ω_p. Equation (16) is analogous to equations of nonlinear optics which are governed by a phase matching condition. The phase matching condition for Eq. (16) is

$$\Delta k\equiv K_F-k_1=0. \quad (17)$$

The secondary magnetic field ΔH is related to the electric field ΔE through Maxwell's equation,

$$\Delta H=\frac{i}{\mu_0\omega}\frac{d\Delta E}{dz}. \quad (18)$$

The solution of wave equation (16) describing the propagation in the forward direction can be written as follows:

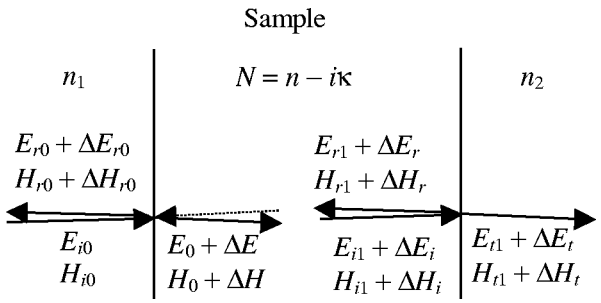

FIG. 3. Notation of electric and magnetic fields at the input and output faces of the sample. In the main part of the paper we assume that the sample is thick enough to allow the temporal windowing of the signal; the backward-propagating wave depicted with a dotted line is not taken into account in the equations for the input interface. However, this wave is taken into account in the Appendix.

$$\Delta E = \delta \exp(-ik_1 z) - \frac{k_0^2 e_0}{k_1^2 - K_F^2} \exp(-iK_F z), \tag{19a}$$

$$\Delta H = \frac{k_1 \delta}{\mu_0 \omega} \exp(-ik_1 z) - \frac{K}{\mu_0 \omega} \frac{k_0^2 e_0}{k_1^2 - K_F^2} \exp(-iK_F z). \tag{19b}$$

The constant δ can be determined from the continuity of the electric and magnetic fields at the input interface ($z=0$),

$$\begin{aligned} &E_{i0} + E_{r0} + \Delta E_{r0} = E_0 + \Delta E, \\ &H_{i0} + H_{r0} + \Delta H_{r0} = H_0 + \Delta H. \end{aligned} \tag{20}$$

The meaning of all fields is explained in Fig. 3. The equilibrium components E_{i0}, E_{r0}, E_0, and H_{i0}, H_{r0}, H_0 fulfill the equilibrium Fresnel equations. The ratio of ΔE_{r0} and ΔH_{r0} is given by the impedance of the surrounding (equilibrium) medium. Thus we are left with the following equations:

$$\Delta E_{r0} = \Delta E, \quad -n_1 \sqrt{\frac{\varepsilon_0}{\mu_0}} \Delta E_{r0} = \Delta H, \tag{21}$$

which allow us to express the coefficient δ. Its substitution back to Eq. (19a) yields

$$\Delta E = \frac{e_0 \exp(-ik_1 z)}{N(\omega) + K_F/k_0} \left[-\frac{1}{n_1(\omega) + N(\omega)} + \frac{1 - \exp(-i\Delta k z)}{N(\omega) - K_F/k_0} \right]. \tag{22}$$

This formula describes the field induced due to the transmission of the THz wave into the nonequilibrium medium ($z=0$) and for the field induced due to propagation in this medium. It is interesting to look what happens in the phase-matched case. In the phase-matching limit Eq. (22) yields

$$\Delta E = \left[-\frac{1}{2N(n_1 + N)} e_0 - \frac{z}{2Nc} (i\omega e_0) \right] \exp(-ik_1 z). \tag{23}$$

The first term in the square bracket can be interpreted as a first order correction to the equilibrium Fresnel formulas. Indeed, if one assumes a time-independent change of the refractive index ΔN of the medium, then the change Δt of the Fresnel transmission coefficient t is equal to

$$\Delta t = \frac{dt}{dN} \Delta N = \left(-\frac{1}{2N(n_1 + N)} \right) \left(\frac{2n_1}{n_1 + N} \right) (2N \Delta N). \tag{24}$$

The product of the second and third term in Eq. (24) is associated with e_0 in expression (23): the second term yields $E_0(z=0^+)$ from $E_0(z=0^-)$, and the third terms stands for the change of the susceptibility $\Delta\chi$.

The second term in the square bracket in Eq. (23) describes the generation of ΔE during the propagation in the medium. It is linear in z as expected for the phase-matching case. This term, considered in Ref. 2, states that the field emitted by the time-dependent polarization during the propagation in the sample, in the near field, is proportional to

$$\Delta E_1 \propto -\frac{\partial \Delta P}{\partial t}. \tag{25}$$

The second term becomes dominant for thick samples. On the other hand, for cases not phase-matched the relative importance of the first term grows. In semiconductors, where the pump pulse is usually absorbed within a few microns, the first (''surface'') term is clearly the leading one.

C. Output interface

The primary wave reflected on the output interface following the Fresnel formulas reads:

$$E_{r1}(\Omega, z) = E_0(\Omega, z=0^+) \exp(-i\Omega N_\Omega L/c) r_{\Omega,2} \times \exp(-i\Omega N_\Omega (L-z)/c),$$

where

$$r_{\Omega,2} = \frac{N(\Omega) - n_2(\Omega)}{N(\Omega) + n_2(\Omega)},$$

and $\Omega = \omega - \omega_p$ (in representation II). The wave equation for the back-propagating secondary wave ΔE_r then takes the form,

$$\frac{d^2 \Delta E_r}{dz^2} + k_1^2 \Delta E_r = -k_0^2 e_{0B} \exp(-iK_B z), \tag{26}$$

where representation II,

$$K_B = -\frac{(\omega - \omega_p) N(\omega - \omega_p)}{c} + \frac{\omega_p}{v_g} - i\alpha,$$

$$e_{0B} = E_0(\omega - \omega_p, z=0^+) \Delta\chi^{(\mathrm{II})}(\omega, \omega_p) \times \exp[-2i(\omega - \omega_p) N(\omega - \omega_p) L/c] r_{\omega - \omega_p, 2}.$$

Reflection of the optical excitation pulse on the output face is weak in usual cases of interest and it is neglected. Note that in this case the pump pulse and the reflected terahertz waves E_{r0} and ΔE_r are counterpropagating, and the phase matching can never be achieved. This is expressed by the first negative term in the definition of K_B. The majority of the energy of the secondary wave generated by the backpropagating wave coming into the detector is delayed by an additional time

$2NL/c$. Taking into account the nonresonant character of this backpropagating term and given the time windowing condition, we omit in the following the right-hand side of Eq. (26). A complete solution of the problem is given in the Appendix and the short discussion there also validates our approach. We are thus left with a very simple wave equation,

$$\frac{d^2\Delta E_r}{dz^2}+k_1^2\Delta E_r=0. \tag{27}$$

The continuity conditions at the output interface, $z=L$, read (see Fig. 3),

$$\begin{aligned} &E_{i1}+\Delta E_i+E_{r1}+\Delta E_r=E_{t1}+\Delta E_t,\\ &H_{i1}+\Delta H_i+H_{r1}+\Delta H_r=H_{t1}+\Delta H_t, \end{aligned} \tag{28}$$

where the equilibrium components E_{i1}, E_{r1}, E_{t1}, and H_{i1}, H_{r1}, H_{t1} fulfill the equilibrium Fresnel equations; ΔE_i and ΔH_i are given by Eqs. (22) and (18) with $z=L$; ΔE_t and ΔH_t are the total transmitted secondary waves,

$$\Delta H_t=n_2\sqrt{\frac{\varepsilon_0}{\mu_0}}\Delta E_t,$$

and ΔE_r and ΔH_r are solutions of the wave equation (27) describing the waves propagating backwards,

$$\Delta E_r=\gamma\exp(ik_1z), \tag{29a}$$

$$\Delta H_r=-\frac{k_1\gamma}{\mu_0\omega}\exp(ik_1z). \tag{29b}$$

The interface conditions allow to eliminate the constant γ and determine ΔE_t. One finds

$$\begin{aligned} \Delta E_t=\frac{\exp(-ik_1L)}{n_2+N}\Bigg[&-\frac{2N}{(N+K_F/k_0)(n_1+N)}\\ &+\frac{1-\exp(-i\Delta kL)}{(N-K_F/k_0)}+\frac{1}{N+K_F/k_0}\Bigg]e_0, \end{aligned} \tag{30}$$

where the argument of the parameters N, n_1, and n_2 which appear explicitly in this expression is the frequency ω. Similarly, in representation I, N and n_0 which appear explicitly have the argument $\omega+\omega_e$. For use later we will formally define a filter function $\Xi=\Delta E_t/e_0$ which represents the relation between the transmitted secondary wave ΔE_t, incident wave E_0 and nonlinear susceptibility $\Delta\chi$,

$$\Delta E_t(\omega,\omega_e)=\Xi(\omega+\omega_e,\omega)E_0(\omega,z=0^+)\Delta\chi^{(\mathrm{I})}(\omega,\omega_e) \tag{31a}$$

in representation I, or

$$\begin{aligned} \Delta E_t(\omega,\omega_p)=&\Xi(\omega,\omega-\omega_p)E_0(\omega-\omega_p,z=0^+)\\ &\times\Delta\chi^{(\mathrm{II})}(\omega,\omega_p) \end{aligned} \tag{31b}$$

in representation II.

D. Discussion

The first term in Eq. (30) corresponds to the first term in expression (22), i.e., to the pulse generated at the input interface which has next passed through the output interface without photoexciting perturbation. The second term is the bulk contribution which strongly depends on the phase-matching condition. Finally, the third term in Eq. (30) has no equivalent in Eq. (22) and it can be identified with a contribution coming from the second interface.

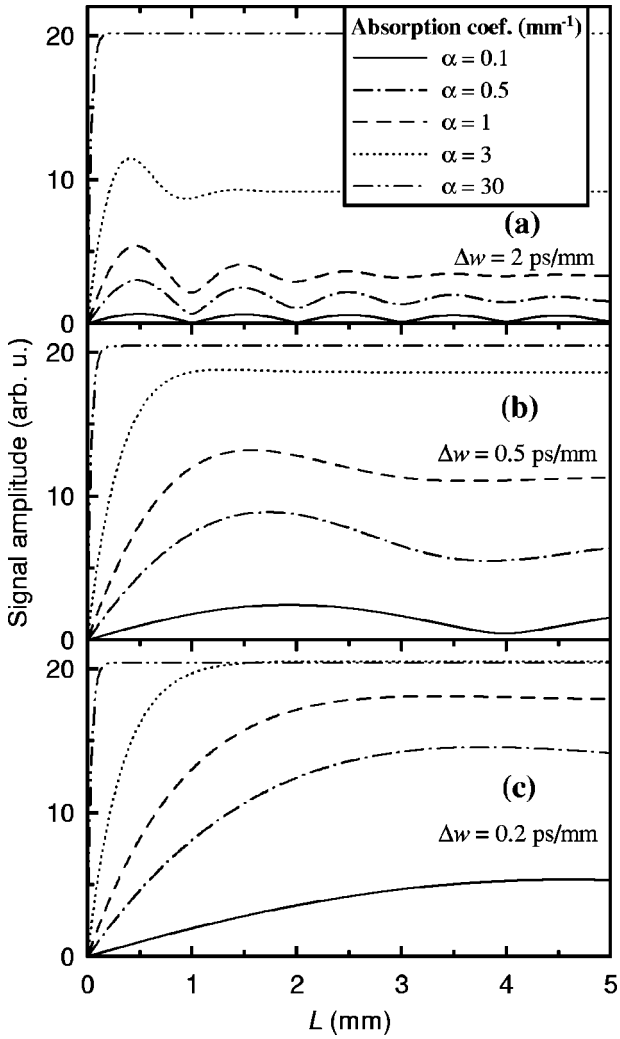

FIG. 4. Amplitude of the secondary wave ΔE_t represented by the quantity $\alpha|\Xi|$ (see text) as a function of the sample length L for different optical absorption coefficients α and for different walk-offs Δw. Parameters: $\omega/\omega_p=2$, $N=1.5$, $n_1=n_2=2$. The curves which are shown were calculated at 1 THz, but as Ξ scales practically linearly with frequency under these conditions, the same curves are obtained for other frequencies.

Assuming that N varies only little with frequency, one can define the pulse walk-off,

$$\Delta w=\frac{N}{c}-\frac{1}{v_g} \tag{32}$$

as a characteristic parameter describing how closely the phase-matching condition is satisfied. The generated amplitude of the secondary wave is plotted in Fig. 4 as a function of the sample length L for different values of the absorption coefficient α and of the walk-off Δw. These plots correspond to experimental situations that are encountered in the study of solvation dynamics in solutions: for a given solvent (characterized by Δw) one looks for a suitable cuvette length and chromophore concentration which linearly scales α. As the magnitude of the nonlinear susceptibility is also expected to

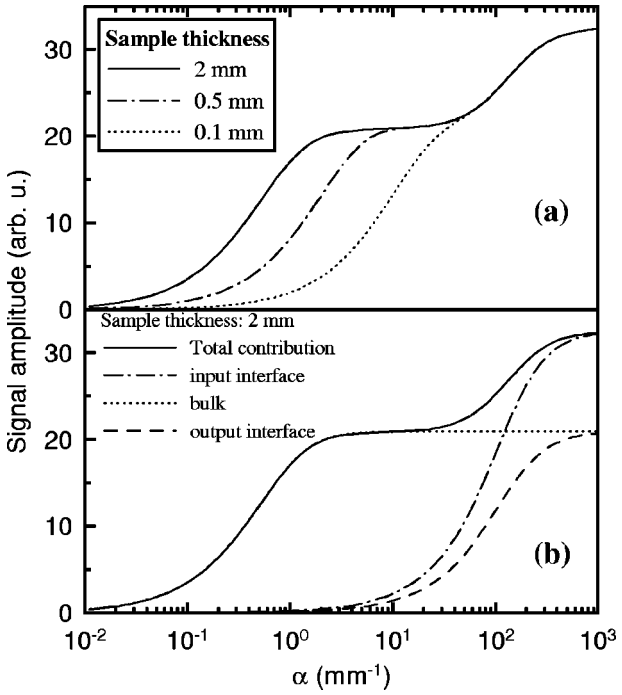

FIG. 5. (a) Amplitude of the secondary wave ΔE_t at 1 THz (represented by the quantity $\alpha|\Xi|$) vs optical absorption coefficients α. Parameters: $\omega/\omega_p=2$, $N=3.5$, $n_1=n_2=1$, $\Delta w=0.2$ ps/mm. (b) Decomposition of the signal amplitude into three contributions which given by the three terms of Eq. (30) and discussed in the text.

be approximately proportional to the chromophore concentration, Fig. 4 in fact shows the product $\alpha|\Xi|$ as a representative function for the measured signal amplitude. If the phase-matching condition is fulfilled (and N is frequency independent), one obtains,

$$\Delta E_t=\left[-\frac{e_0}{(n_1+N)(n_2+N)}-\frac{L}{c(N+n_2)}(i\omega e_0)+\frac{e_0}{2N(n_2+N)}\right]\exp(-ik_1L). \tag{33}$$

In the case of a solution in cuvette, $n_1\approx N$; then, the first and the third (''surface'') terms partially compensate for each other and the bulk (phase-matched) contribution is thus the leading one as it can be seen in Fig. 4; the amplitude practically vanishes for $L=0$.

In contrast, only the first term of Eq. (30) will contribute in semiconductors where the pump beam is usually absorbed within a few microns near the input interface because the parameters K_F and Δk have very high imaginary parts,

$$\Delta E_t\approx-\frac{2N\exp(-ik_1L)e_0}{(n_2+N)(N+K_F/k_0)(n_1+N)}. \tag{34}$$

This is illustrated in Fig. 5, where the signal amplitude $|\alpha\Xi|$ is plotted versus the absorption coefficient. Here the multiplication of Ξ by the absorption coefficient over several decades is not completely justified as in the previous case: we take it as the simplest approximation and, consequently, the curves show the expected behavior only schematically. The situation encountered in solutions corresponds to the initial increase of the signal amplitude where the bulk term is dominant and the surface terms counterbalance each other. The semiconductors or other highly absorbing materials are represented by the second increase of the signal amplitude which is independent of the sample thickness and where the term coming from the first surface becomes dominant while the sum of the remaining terms vanish [Fig. 5(b)].

V. EXPERIMENTAL SCHEMES

In Sec. III we introduced two possibilities of 2D temporal scanning in OPTP experiments which lead to two representations of the THz secondary wave emitted by the sample due to the photoexcitation [Eqs. (30) and (31a), (31b)].

A. Representation I

In the case of representation I, one performs a 2D scan using D2 (τ) and D1 (τ_e) delay lines. The reference measurement is done with the pump beam suppressed and using the D2 delay line. D3 is fixed in both experiments in the same position. Taking into account Eqs. (2), (12a), and (31a) one finds for the measured signal (see Fig. 1),

$$\frac{\Delta E^D(\omega,\omega_e)}{E^D_{\rm ref}(\omega)}=\frac{\psi_2(\omega_e+\omega)}{\psi_2(\omega)}\frac{\psi_1(\omega_e+\omega)}{\psi_1(\omega)}\times\frac{\Xi(\omega_e+\omega,\omega)\Delta\chi(\omega,\omega_e)}{T_{\rm ref}(\omega)}\frac{E_0(\omega)}{E_0(\omega)}, \tag{35}$$

where $T_{\rm ref}(\omega)$ is the reference transmission function of the nonexcited sample ψ_1 accounts for the spatiotemporal transformations of the THz pulse between the sample and the detector, and, in the case of a sample in a cuvette, also for the propagation through the output window of the cuvette. This last contribution is simple to describe if the characteristics of the cuvette material are known, namely, it simplifies owing to the reference measurement into a pure phase factor if the dispersion of the cuvette in the THz range is negligible,

$$\frac{\psi_{\rm cuv}(\omega_e+\omega)}{\psi_{\rm cuv}(\omega)}\approx\exp(-i\omega_e n_2 d/c), \tag{36}$$

where d is the cuvette output window thickness. Concerning the spatiotemporal transformations, it is necessary to avoid them after the sample by following the protocol for the emission experiment described in Ref. 27, i.e., the transmitted on-axis THz waveform $E^D(\tau,\tau_e)$ is measured in the far field without any additional focusing optics. The relevant part of the instrumental function ψ_1 accounts for the near field–far field transformation and it is proportional to frequency,

$$\frac{\psi_{\rm air}(\omega_e+\omega)}{\psi_{\rm air}(\omega)}\approx\frac{\omega_e+\omega}{\omega}\exp(-i\omega_e D/c), \tag{37}$$

where D is the distance between the output face of the cuvette (sample) and the sensor. The sum of the two large linear phase factors from Eqs. (36) and (37) corresponds to the time shift of the resulting susceptibility by $t'=(n_2d+D)/c$ in the variable τ_e. This follows from the definition of $\tau_e=t-t_e$, where t is the time of the measurement and t_e is the time of the pump pulse arrival into the sample. No signal of interest can be measured for $\tau_e<t'$. One can thus cancel

these phase factors provided that the origin of τ_e is defined in the experiment as the time delay when the first signal related to the optical excitation has been detected.

Although the terms $E_0(\omega)$ in Eq. (35) cancel out, they are formally written here, since the finite extent of the THz spectrum limits the experimentally accessible range. This is discussed in more detail in Sec. V C.

Finally, ψ_2 is the spectral responsivity of the sensor. The relation between the true THz waveform incident on the detector and the detected waveform has already been described in the case of the electro-optic sampling; in the most general case, the detection spectral response function is given by Eq. (57) in Ref. 26. Under usual experimental conditions where the bandwidth $\Delta\omega_L$ of the sampling optical pulse is much smaller than its carrier frequency ω_L the response function $\psi_2(\Omega)$ of the detection system writes

$$\psi_2(\Omega)=\left[\int_{-\infty}^{\infty}E_L^*(\omega')E_L(\omega'-\Omega)d\omega'\right]\times\chi_{\mathrm{eff}}^{(2)}(\omega_L;\Omega,\omega_L-\Omega)\times\frac{\exp\left(i\frac{\Omega}{c}l\Delta n(\Omega,\omega_L)\right)}{i\frac{\Omega}{c}\Delta n(\Omega,\omega_L)}\frac{2n}{n+1}, \tag{38}$$

where Ω is a general frequency variable. The first term in Eq. (38) is the frequency domain autocorrelation of the optical electric field E_L, which describes how the measured THz waveform is broadened due to finite temporal length of the optical sampling pulse. The second term corresponds to the Pockels coefficient dispersion in the THz frequency range. The third term describes the waveform distortion due to the dispersion of the sensor (l is the sensor thickness) and due to the velocity mismatch, which is incorporated in the difference between the group refractive index n_g of the sampling pulse, and the THz refractive index n,

$$\Delta n(\Omega,\omega_L)=n(\Omega)-n_g(\omega_L)=n(\Omega)-n(\omega_L)-\omega_L\frac{dn(\omega_L)}{d\omega_L}. \tag{39}$$

Finally, the fourth term of Eq. (38) accounts for the Fresnel losses on the input face of the sensor.

All the required quantities can be experimentally determined for a given Pockels crystal, thus ψ_2 can be calculated. However, as ψ_2 contains a sum frequency in its argument it is necessary to measure $\psi_2(\Omega)$ in a spectral range exceeding the available THz bandwidth in order not to reduce the accessible frequency range of $\Delta\chi(\omega_e,\ \omega)$.

The nonequilibrium susceptibility can be directly calculated from Eq. (35),

$$\Delta\chi(\omega,\omega_e)=\frac{T_{\mathrm{ref}}(\omega)}{\Xi(\omega_e+\omega,\omega)}\frac{\Delta E^D(\omega,\omega_e)}{E^D_{\mathrm{ref}}(\omega)}\times\frac{\omega\psi_2(\omega)}{(\omega_e+\omega)\psi_2(\omega_e+\omega)}. \tag{40}$$

The presence of the sum frequency factor in the argument of the sensor response function $\psi_2(\omega_e+\omega)$ is closely related to the experimental protocol associated to representation I. For a given position of D1 (scan of t_e) and D2 (scan of t_p) one point of the nonequilibrium THz waveform is measured. We now fix the pump pulse arrival (D1) and move the delay line D2; this corresponds to a waveform measurement as the probe–sampling distance $(t-t_p)$ is scanned. However, by moving D2, the pump–probe distance (t_p-t_e) is changed at the same time. Consequently, each point of the waveform obtained using this experimental protocol is influenced differently by the pump pulse. The factor $\psi_2(\omega_e+\omega)$ takes this fact into account. Similar arguments can be drawn for Eq. (35) to justify the term $\psi_1(\omega_e+\omega)$ describing the spatiotemporal transformations.

The main advantages of this representation are that (i) the shape of the incident waveform is completely canceled out thanks to the reference measurement, and that (ii) once the sensor is properly characterized, the evaluation of the nonequilibrium susceptibility is straightforward for all subsequent measurements. On the other hand, it should be carefully checked that the measurements are really performed in the far field. The major disadvantage of this method is that the detected THz beam is not focused, thus the S/N ratio is significantly decreased. In order to improve the signal, it would be necessary to use focusing optics (paraboloidal or ellipsoidal mirrors or FIR spherical lenses). However, this would complicate very significantly the form of the response function ψ_1. It can still be evaluated analytically within Gaussian-beam approximation,[23] but this approximation is not always valid within the required precision; the spherical aberration significantly broadens the THz pulses and paraboloidal and ellipsoidal profiles can lead to departures from Gaussian-type propagation characteristics. On the other hand, numerical calculations within the scalar diffraction theory[31] always require assumptions about the transverse profile of the THz beam and do not allow a simple analytical treatment based on Eq. (1) using a temporal convolution with a response function; the response function will in fact depend on the spatial profile. Moreover, the calculations are very sensitive to the geometrical arrangement (all distances and apertures of used optics).

B. Representation II

Let us turn now our attention to the second possibility (representation II) for which one needs to perform the 2D scan using D3 (τ) and D1 (τ_p) delay lines. The reference measurement is done with the pump beam suppressed and using the D3 delay line. D2 is fixed in both experiments in the same position. Taking into account Eqs. (2), (12b), and (31b) one finds for the measured signal,

$$\frac{E^D(\omega,\omega_p)}{E^D_{\mathrm{ref}}(\omega)}=\frac{\psi_2(\omega)}{\psi_2(\omega)}\frac{\psi_1(\omega)}{\psi_1(\omega)}\frac{\Xi(\omega,\omega-\omega_p)\Delta\chi(\omega,\omega_p)}{T_{\mathrm{ref}}(\omega)}\times\frac{E_0(\omega-\omega_p)}{E_0(\omega)}. \tag{41}$$

The meaning of the symbols is analogous to that in Eq. (35). The response functions ψ_1 and ψ_2 describing the propagation after the sample are eliminated. Their absence in this expression allows one to choose any experimental arrangement behind the sample, and, consequently to focus the THz power into the sensor. On the other hand, it is necessary to determine precisely the waveform incident on the sample. It implies replacing the sample by the sensor, to measure the waveform (denoted as E_M), and subtract the influence of the sensor using the function ψ_2. Then Eq. (41) yields for the nonequilibrium susceptibility the following formula:

$$\Delta\chi(\omega,\omega_p)=\frac{T_{\mathrm{ref}}(\omega)}{\Xi(\omega,\omega-\omega_p)}\frac{E^D(\omega,\omega_p)}{E^D_{\mathrm{ref}}(\omega)}\frac{E_M(\omega)\psi_2(\omega-\omega_p)}{E_M(\omega-\omega_p)\psi_2(\omega)}. \tag{42}$$

Similarly as in expression (40) we canceled the phase factors,

$$\exp(-i\omega_p(n_1 d+\Delta D)/c),$$

where d is the thickness of the input window of the cuvette and ΔD is a possible distance between the position of the input face of the sensor and of the sample. Here the phase factor can be determined if the experimental setup allows to minimize the uncertainty in the determination of ΔD.

If the experimental THz setup is sufficiently stable in time, it is possible to determine the complex spectrum of the waveform E_0 only once for a whole set of nonequilibrium measurements. It is obvious that the precision of this determination is crucial. In order to minimize the influence of the sensor, it is possible to use a very thin Pockels crystal for the detection, e.g., a thin $\langle 110\rangle$ ZnTe crystal[25] in an optical contact with a thicker one in $\langle 100\rangle$ orientation so as to avoid multiple Fabry–Pérot reflections. Then the spectrum $\psi_2(\omega)$ is much flatter[32] and the evaluation is less sensitive to experimental errors.

Note that in usual optical pump–probe experiments, where relatively slow changes are measured compared to the carrier frequency of the optical probe pulse (i.e., $\omega_p \ll \omega$), the influence of the incident pulse shape is canceled out in Eq. (41), one-dimensional FT can be performed, and a slowly-varying time-dependent susceptibility $\Delta\chi(\tau_p, \omega)$ can be introduced. It should be noted that this is also the case for OPTP experiments if one measures only slow dynamics compared to the THz pulsewidth ($\omega_p \ll \omega$).

C. Accessible data

In both presented experimental protocols, one part of the instrumental functions is eliminated. For D1–D2 scans we need not take care about the propagation before the sample, however we do have to account for the propagation after the sample. The opposite is true for D1–D3 scans; the waveform before the sample has to be determined, while the propagation after the sample is absent in the formulas. The sensor characteristics have to be elucidated for both experiments.

Both possibilities of 2D scans are schematically represented in Fig. 6. Figures 6(a) and 6(b) represent the ranges of time delays which need to be scanned.

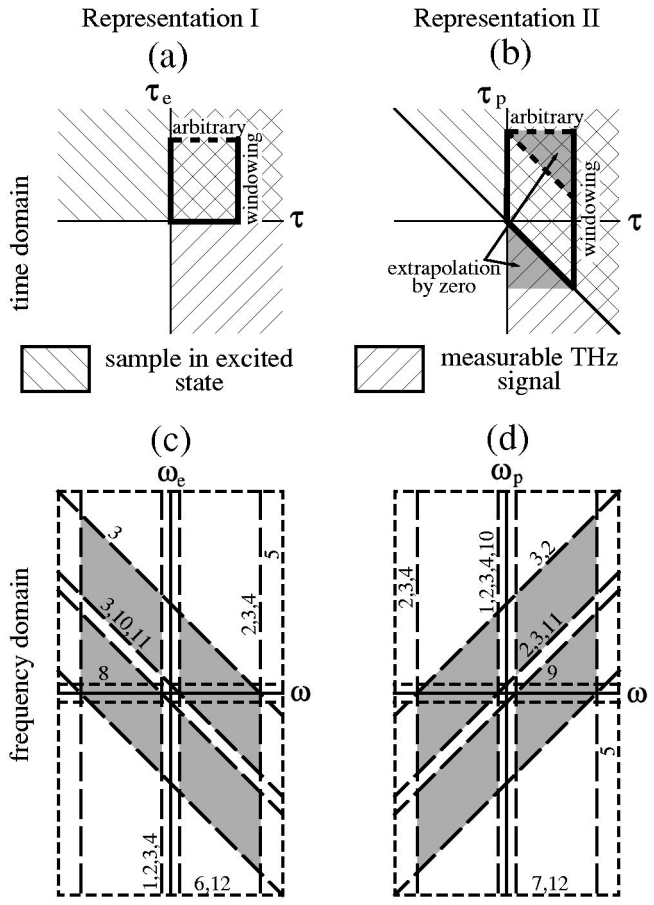

FIG. 6. Upper part: 2D time-domain scans to be performed; (a) representation I; (b) representation II. Lower part: accessible ranges in the corresponding 2D Fourier spaces for representation I (c) and representation II (d). Gray shadowing represents areas where $\Delta\chi$ can be experimentally obtained (see text). Delimiting lines are related to the temporal windowing (1), spectrum of incident pulse (2), sensor (3), sample in equilibrium state (4), sampling rates in τ, τ_e, and τ_p (5), (6), and (7), scan lengths in τ_e and τ_p (8) and (9), filter function Ξ (10), diffraction (11), and pump pulse length (12).

For representation I [Fig. 6(a)], τ and τ_e are connected to the displacement of D2 and D1, respectively; the area of interest containing the complete information is rectangular. It is limited in τ owing to the temporal windowing; on the other hand, sufficiently long scans in τ_e should be performed (until the signal related to the pump pulse vanishes). The origin of τ_e was chosen as the time delay when the first signal related to the optical excitation has been detected.

The rectangle transforms into a parallelogram in representation II [Fig. 6(b)]; the pump pulse approaches the sample at $\tau_e=\tau_p+\tau=0$ [cf. Eq. (8)], i.e., the data below the diagonal line $\tau_p=-\tau$ cannot be influenced by the pump and their value is zero by definition. For large values of $\tau_p+\tau$ the signal due to the excitation is supposed to vanish. Thus, as shown in Fig. 6(b), the parallelogram can be completed by two triangles filled by zeroes to obtain a rectangle suitable for 2D FT.

Figures 6(c) and 6(d) show schematically the frequency ranges where nonequilibrium susceptibility $\Delta\chi$ can be calculated. The susceptibility at negative frequencies is calculated using the properties $\Delta\chi(\omega,\omega_e)=\Delta\chi^*(-\omega,-\omega_e)$ and $\Delta\chi(\omega,\omega_p)=\Delta\chi^*(-\omega,-\omega_p)$. The experimentally acces-

sible areas are defined as frequency ranges where both the signal spectrum E^D and the reference spectrum E^D_{ref} exceed the noise level. They are delimited by a set of lines plotted in Figs. 6(c) and 6(d) which are characteristic for the experimental setup or its parts and which are obtained from Eqs. (35) and (40) for representation I, and from Eqs. (41) and (42) for representation II.

With representation I [Fig. 6(c)], the accessible range is in principle defined by the sampling rates in τ and τ_e (high-frequency limit) and by the scan lengths in τ and τ_e (low-frequency limit). It can be reduced further by all the factors which appear at the right-hand side of Eq. (35); e.g., the spectrum of the incident THz pulse $E_0(\omega)$ cancels out in this expression, however, it can still diminish the spectral range where $E^D(\omega,\omega_e)$ and $E^D_{\mathrm{ref}}(\omega)$ can be experimentally obtained. The principal factors that can decrease the low- and high-frequency limits of the measurement in ω [vertical lines in Fig. 6(c)] are the spectrum of the incident pulse $E_0(\omega)$, the sensitivity of the sensor $\psi_2(\omega)$, and the equilibrium properties of the sample $T_{\mathrm{ref}}(\omega)$; in addition, the low-frequency part of the spectrum can be limited by the temporal windowing. The terms which contain the sum argument $\omega+\omega_e$ are then at the origin of diagonal delimiting lines in Fig. 6(c). The most important factor here is the upper limit of the spectral sensitivity of the sensor which, due to its diagonal character, reduces the accessible area very drastically—by more then one half. The filter function Ξ and the propagator ψ_1 are approximately linear in $\omega+\omega_e$, so that they can in principle influence the low-frequency diagonal limit shown in Fig. 6(c).

Similar discussion can be drawn for representation II; the accessible spectral area is plotted in Fig. 6(d). While the experimenter can influence the positions of short-dashed lines plotted in Figs. 6(c) and 6(d) (e.g., lengths of scans and sampling rate), those of long-dashed lines are given by characteristics of the experimental setup (sensor, emitter, opacity of the sample, etc.) and the reduction of the accessible area due to these lines cannot in principle be avoided.

Our approach allows to conceive another interesting experimental protocol. We take as a reference another 2D scan in different conditions. Different conditions can mean, e.g., a different temperature or a different excitation wavelength; it can be interesting especially with semiconductors to compare the dynamics of photoexcited carriers generated just above or well above the band gap. It is then possible to recover very precisely (without knowledge of any instrumental function) the ratio of the spectra of nonlinear susceptibilities,

$$\frac{\Delta\chi_1(\omega,\omega_p)}{\Delta\chi_2(\omega,\omega_p)}=\frac{E_1^D(\omega,\omega_p)}{E_2^D(\omega,\omega_p)}, \tag{43a}$$

$$\frac{\Delta\chi_1(\omega,\omega_e)}{\Delta\chi_2(\omega,\omega_e)}=\frac{E_1^D(\omega,\omega_e)}{E_2^D(\omega,\omega_e)}, \tag{43b}$$

where indices 1 and 2 denote the different experimental conditions. It is then possible to follow easily the changes of nonlinear susceptibility as a function of another external parameter. Note, however, that if the external parameter can simultaneously change the equilibrium properties of the sample—this, for example, is the case of the temperature—it is necessary to take it into account through a modification of Ξ.

VI. CONCLUSION

We have solved the problem of the propagation of THz electromagnetic transients in photoexcited media up to the first order. We have shown that using a 2D FT approach one can derive an explicit formula for the 2D spectrum of nonlinear susceptibility describing the ultrafast dynamics of the medium after the optical excitation. The results can be applied both to optically highly absorbing media, where Fresnel-type interface effects dominate, and to media with lower optical absorption where the phase-matching condition in the bulk becomes important.

We have proposed two experimental schemes and discussed their advantages and drawbacks. One of the instrumental functions ψ_0 or ψ_1 is canceled out from the expressions for $\Delta\chi$ owing to the 2D FT approach. All the equilibrium characteristics of the sample, cuvette, and sensor need to be preliminarily determined and spectral filtering functions appearing in the final expressions (40) and (42) should be plotted and examined. It is then possible to determine the spectral range where susceptibility can be determined from the terahertz experiment. The relative variation of nonlinear susceptibility as a function of another external parameter can be determined without knowledge of any instrumental function. In this respect, our approach appears to be more convenient than alternative time-domain treatments, where all the instrumental functions ψ_0, ψ_1, and ψ_2 have to be experimentally determined. Moreover, unlike the numerical time-domain treatment (FDTD), the proposed scheme allows for a direct evaluation of $\Delta\chi$ without an *a priori* model.

ACKNOWLEDGMENTS

The authors wish to thank P. Jungwirth and P. Slavíček of the J. Heyrovsky Institute of Physical Chemistry, Prague; B. Schmidt of Freie Universität Berlin for helpful discussions; and J. Novotney for revising the manuscript. The support from the Ministry of Education of the Czech Republic (Project No. LN00A032) and from the Volkswagen Stiftung (Grant No. I/75908) is also acknowledged.

APPENDIX: SOLUTION OF THE WAVE EQUATION WITHOUT TEMPORAL WINDOWING

Here we solve the problem of propagation in a photoexcited medium without the temporal windowing of the THz signal, i.e., all the internal reflections in the sample are taken into account. The remaining assumptions are retained, namely, $\Delta E \ll E_0$, expressed by Eqs. (13) and (14). The definitions of the symbols given in Eqs. (16) and (26) are used. The wave equation for the total secondary THz field ΔE in the sample writes

$$\frac{d^2\Delta E}{dz^2}+k_1^2\Delta E=-k_0^2 e_0[A_F\exp(-iK_F z) + A_B\exp(-iK_B z)], \tag{A1}$$

where the parameters

$$A_F=\sum_{j=0}^{\infty}(r_1r_2)^j\exp[-2i(\omega-\omega_p)N(\omega-\omega_p)jL/c],$$

$$A_B=\frac{1}{r_1}\sum_{j=1}^{\infty}(r_1r_2)^j\exp[-2i(\omega-\omega_p)N(\omega-\omega_p)jL/c],$$

describe the sum of internal reflections of the primary wave in the sample. The general solution of the wave Eq. (A1) writes,

$$\Delta E=\gamma\exp(ik_1z)+\delta\exp(-ik_1z)-\sum_{m=F,B}\frac{k_0^2e_0A_m}{k_1^2-K_m^2}\exp(-iK_mz). \tag{A2}$$

The relations between the secondary wave reflected by the structure (ΔE_{r0}), transmitted by the structure (ΔE_t) and the constants δ and γ are given through the field continuity at the interfaces,

$$\begin{aligned}&\Delta E_{r0}=\Delta E(z=0),\\&-k_0n_1\Delta E_{r0}=\mu_0\omega\Delta H(z=0),\\&\Delta E(z=L)=\Delta E_t,\\&\mu_0\omega\Delta H(z=L)=k_0n_2\Delta E_t.\end{aligned} \tag{A3}$$

After introducing ΔE given by Eq. (A2) and the corresponding magnetic field ΔH calculated using Eq. (18) into the system of equations (A3) one finds

$$\Delta E_t=\left\{\sum_{m=F,B}\left[\left(1-\frac{2N}{n_1+N}\right)\frac{1-\exp(-i(K_m+k_1)L)}{N+K_m/k_0}\times\frac{1-\exp(-i(K_m-k_1)L)}{N-K_m/k_0}\right]\frac{A_me_0\exp(-ik_1L)}{n_2+N}\right\}\times\sum_{j=0}^{\infty}\left(\frac{N-n_1}{N+n_1}\frac{N-n_2}{N+n_2}\right)^j\exp(-2ik_1jL). \tag{A4}$$

The last sum accounts for the multiple internal reflections of the generated secondary pulses. The internal reflections of the primary wave are encoded into A_m coefficients. The remaining terms thus describe the generation in various orders of these reflections.

The exponential term containing the sum K_m+k_1 can never become phase matched for either forward ($m=F$) or backward wave ($m=B$); this exponential thus only describes a higher order term from the point of view of temporal windowing. The first-order terms (direct pass of the beam) contain only contributions given in Eq. (30),

$$\Delta E_{t,1,F}=\left[\left(1-\frac{2N}{n_1+N}\right)\frac{1}{N+K_F/k_0}+\frac{1-\exp(-i(K_F-k_1)L)}{N-K_F/k_0}\right]\frac{e_0\exp(-ik_1L)}{n_2+N}. \tag{A5}$$

The lowest-order terms coming from the backward propagation read,

$$\Delta E_{t,1,B}=\left[\left(1-\frac{2N}{n_1+N}\right)\frac{1}{N+K_B/k_0}+\frac{1-\exp(-i(K_B-k_1)L)}{N-K_B/k_0}\right]\frac{e_0r_2\exp(-ik_1L)}{n_2+N}\times\exp[-2i(\omega-\omega_p)N(\omega-\omega_p)L/c]. \tag{A6}$$

In principle, these terms are delayed in time with respect to those of Eq. (A5) as the propagator term in Eq. (A6) is roughly equal to $-3ik_1L$. This validates for the majority of cases our approximation expressed by Eq. (27). The second term in the square bracket of Eq. (A6) can become resonant only in a hypothetical case when the phase-matching condition (17) is satisfied and, simultaneously, the primary field has a nonvanishing static component ($\omega=\omega_p$). On the other hand, if we are far from the phase matching condition, the generated signal based on this term will be small. At the same time the nonvanishing positive argument of the exponential term $\exp(-i(K_B-k_1)L)$ will decrease the effective time delay of this contribution. The interpretation of this contribution is the following: out of the phase-matching the back-propagating primary wave generates in the bulk a small part of the secondary wave with an opposite propagation direction (i.e., this secondary wave propagates directly forward after generation). This secondary wave then comes into the detector at intermediate times (with a delay between NL/c and $3NL/c$), thus the temporal windowing procedure cannot be strictly defined. Consequently, a small systematic error is introduced into the treated data if Eq. (30) and the time-windowing are applied in this case.

[1] M. C. Nuss, and J. Orenstein, *Terahertz Time-Domain Spectroscopy, in Millimeter and Submillimeter Wave Spectroscopy of Solids*, edited by G. Grüner (Springer-Verlag, Berlin, 1998), Chap. 2, p. 7.
[2] J. T. Kindt and C. A. Schmuttenmaer, J. Chem. Phys. **110**, 8589 (1999).
[3] M. C. Nuss, D. H. Auston, and F. Capasso, Phys. Rev. Lett. **58**, 2355 (1987).
[4] B. I. Greene, J. F. Federici, D. R. Dykaar, A. F. J. Levi, and L. Pfeiffer, Opt. Lett. **16**, 48 (1991).
[5] P. N. Saeta, J. F. Federici, B. I. Greene, and D. R. Dykaar, Appl. Phys. Lett. **60**, 1477 (1992).
[6] D. C. Flanders, B. N. Arnett, and N. F. Scherer, IEEE J. Sel. Top. Quantum Electron. **4**, 353 (1998).
[7] M. Schall and P. U. Jepsen, Opt. Lett. **25**, 13 (2000).
[8] S. S. Prabhu, S. E. Ralph, M. R. Melloch, and E. S. Harmon, Appl. Phys. Lett. **70**, 2419 (1997).
[9] M. C. Beard, G. M. Turner, and C. A. Schmuttenmaer, Phys. Rev. B **62**, 15764 (2000).
[10] S. E. Ralph, Y. Chen, J. Woodall, and D. McInturff, Phys. Rev. B **54**, 5568 (1996).
[11] M. C. Beard, G. M. Turner, and C. A. Schmuttenmaer, J. Appl. Phys. **90**, 5915 (2001).
[12] R. D. Averitt, G. Rodriguez, J. L. W. Siders, S. A. Trugman, and A. J. Taylor, J. Opt. Soc. Am. B **17**, 327 (2000).
[13] G. Haran, W.-D. Sun, K. Wynne, and R. M. Hochstrasser, Chem. Phys. Lett. **274**, 365 (1997).
[14] R. McElroy and K. Wynne, Phys. Rev. Lett. **79**, 3078 (1997).
[15] M. C. Beard, and C. A. Schmuttenmaer, J. Chem. Phys. **114**, 2903 (2001).
[16] D. Grischkowsky, S. Keiding, M. Van Exter, and Ch. Fattinger, J. Opt. Soc. Am. B **7**, 2006 (1990).
[17] L. Duvillaret, F. Garet, and J.-L. Coutaz, IEEE J. Sel. Top. Quantum Electron. **2**, 739 (1996).
[18] Ch. Fattinger and D. Grischkowsky, Appl. Phys. Lett. **53**, 1480 (1988).
[19] Q. Wu, M. Litz, and X.-C. Zhang, Appl. Phys. Lett. **68**, 2924 (1996).

[20] P. Kužel and J. Petzelt, Ferroelectrics **239**, 949 (2000).
[21] M. Van Exter, Ch. Fattinger, and D. Grischkowsky, Opt. Lett. **14**, 1128 (1989).
[22] R. W. Ziolkowski and J. B. Judkins, J. Opt. Soc. Am. A **9**, 2021 (1992).
[23] P. Kužel, M. A. Khazan, and J. Kroupa, J. Opt. Soc. Am. B **16**, 1795 (1999).
[24] D. You and P. H. Bucksbaum, J. Opt. Soc. Am. B **14**, 1651 (1997).
[25] H. J. Bakker, G. C. Cho, H. Kurz, Q. Wu, and X.-C. Zhang, J. Opt. Soc. Am. B **15**, 1795 (1998).
[26] G. Gallot and D. Grischkowsky, J. Opt. Soc. Am. B **16**, 1204 (1999).
[27] H. Němec, A. Pashkin, P. Kužel, M. Khazan, S. Schnüll, and I. Wilke, J. Appl. Phys. **90**, 1303 (2001).
[28] M. C. Beard, G. M. Turner, and C. A. Schmuttenmaer, J. Am. Chem. Soc. **122**, 11541 (2000).
[29] M. C. Beard, G. M. Turner, and C. A. Schmuttenmaer, J. Phys. Chem. A **106**, 878 (2002).
[30] L. Duvillaret, F. Garet, J.-F. Roux, and J.-L. Coutaz, IEEE J. Sel. Top. Quantum Electron. **7**, 615 (2001).
[31] E. Budiarto, N.-W. Pu, S. Jeong, and J. Bokor, Opt. Lett. **23**, 213 (1998).
[32] G. Gallot, J. Zhang, R. W. McGowan, T.-I. Jeon, and D. Grischkowsky, Appl. Phys. Lett. **74**, 3450 (1999).